



## Design and modeling of a hybrid soft-rigid hand exoskeleton for poststroke rehabilitation

Legeng Lin, Fuhai Zhang\*, Lei Yang, Yili Fu

The State Key Laboratory of Robotics and System, Harbin Institute of Technology, Harbin 150001, China



### ARTICLE INFO

**Keywords:**

Rehabilitation robotics  
Hybrid soft-rigid mechanism  
Hand exoskeletons  
Nonlinear modeling

### ABSTRACT

Poststroke patients' need for hand rehabilitation is urgent since hand plays a significant role in people's activities of daily life (ADLs). Contrast to traditional rigid devices with excessive stiffness and soft devices lacking well-understood models, we present a hybrid soft-rigid exoskeleton (HSRexo) for poststroke hand rehabilitation adopting the simplified three-layered sliding spring (sTLSS) mechanism that combines the intrinsic compliance and comprehensible kinematics. The compliant spring blades in the sTLSS mechanism make it possible to compactly actuate three natural flexion/extension of finger joints by only 1° of freedom (DOF). To deal with the nonlinear deformation of soft elastic elements, the modeling of the sTLSS mechanism is proposed by the pseudo-rigid-body model (PRBM) method to achieve comprehensible kinematics and optimize design parameters. Finally, the simulation and preliminary prototyping demonstrate the accuracy of the model and the compliant natural flexion/extension joint angle of the HSRexo design due to the modeling and optimization of the sTLSS mechanism.

### 1. Introduction

The World Health Organization (WHO) estimated that 15 million people suffer from stroke every year [1]. Almost 80% of survivors of stroke have disabilities on limbs [2], in which the disorder of hand is more severe since hands play the most important role in normal activities of daily life (ADLs). The traditional rehabilitation assisted by physiotherapists has the disadvantages of intensive labor, low efficiency, and high cost [3]. On the contrary, the rehabilitation assisted by robots has the advantages of sparse labor, long duration, good repeatability, and task orientation. It is approved in a clinical survey that robot-assisted stroke rehabilitation can effectively improve the result of rehabilitation [4]. The objective of robot-assisted rehabilitation is to stimulate the related motion system nerves on the cerebral cortex, strengthen the weak muscles, and then recover the motion function of the hand to perform ADLs.

Since the human hand has as many as 20° of freedom (DOFs) but with coupled relation in hand motion, the robot-assisted hand rehabilitation can be simplified to achieve grasp motion task. Therefore it is popular for hand exoskeletons to achieve the functional degree of freedom (fDOF) which means that complex movement patterns can be generalized and achieved by less complex actuation strategies [5].

Besides, the hand exoskeleton directly contacts with human hand. Therefore, under the premise of ensuring safety, the mechanism also needs to meet the requirements of wearability, comfortability, and portability. Hand exoskeleton has to consider the alignment between exoskeleton joints and human joints to achieve compatibility.

State-of-the-art hand exoskeleton devices can be mainly divided into two kinds: rigid devices (e.g., linkage, pinion & rack) and soft devices (e.g., elastomer, pneumatic, hydraulic). Rigid linkage [6–8] and pinion & rack mechanisms [9] are popular choices because their flexion/extension motions are realized through kinematic chains adopted from the traditional mechanical design. The advantages of rigid devices are accurate kinematics, robust force control, and high efficiency of power transmission. However, rigid devices suffer from inherent excessive stiffness, bulky size and weight, which are unsafe and uncomfortable for patients. To achieve compatibility with human fingers, some of the rigid devices add elastic elements like spring into the traditional linkage mechanism [10,11] to improve compliance of the mechanism. Others use passive mechanisms to compensate for the misalignment [12]. But, as a result, they lead to more complexity and weight which are more unsuitable for the hand exoskeleton on the distal part of human upper limb.

Another way is using soft elements to design the hand exoskeleton.

\* Corresponding author.

E-mail address: [zfhhit@hit.edu.cn](mailto:zfhhit@hit.edu.cn) (F. Zhang).

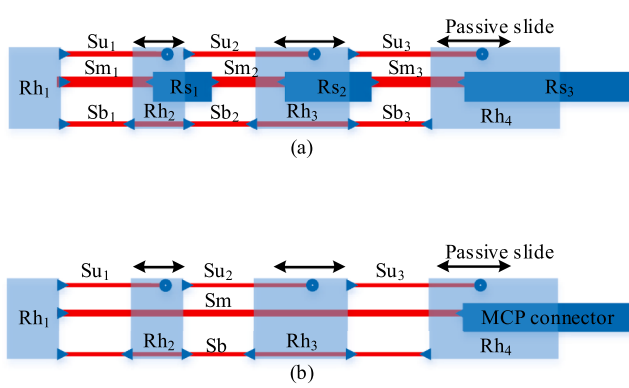
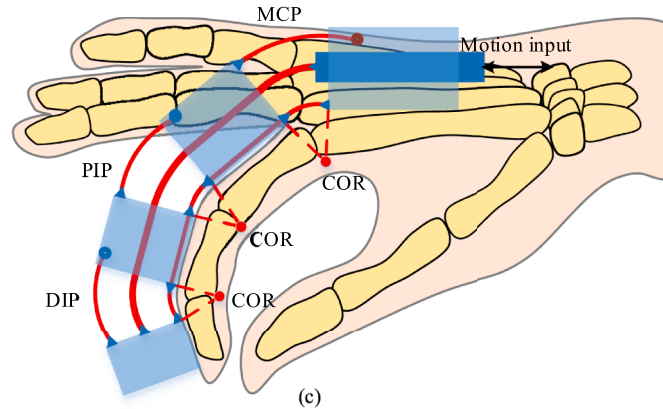


**Fig. 1.** TLSS and sTLSS mechanism. (a) TLSS mechanism. (b) sTLSS mechanism. (c) The corresponding relationship between sTLSS mechanism and human finger. (In these abbreviations, “Rh” means “rigid holder”, “Rs” means “rigid slider”, “Su” means “upper spring”, “Sm” means “middle spring”, “Sb” means “bottom spring”, and “COR” means “center of rotation”).

Soft devices made entirely from fluids-powered soft elastomer [13] or cable-driven textiles [14,15] can generate powerful output with inherent compliance. Therefore, soft elastomer has the natural advantage of compatibility with human body for wearable application [16]. However, the model of soft elastomer is not well-understood because its intrinsic deformation is complex, nonlinear, and highly compliant [16, 17], which increases the difficulty of motion control. Thus, modeling and predicting their behavior is a challenge due to uncertainties [18,19]. Cable-driven textiles can remotely arrange the actuator, optimize the distribution of inertia, and improve the compliance. However, it has the disadvantages of low efficiency, backslash, hysteresis, and inaccurate force transmission [20].

As a result, hybrid soft-rigid exoskeletons use deformable materials like cable-driven textiles [21], inflatables [22], compression springs [23], and spring blades [24–26] in combination with a rigid frame. They combine the compliance of soft elements and the accuracy of rigid elements. For example, in the design of Single-size Semi-soft Assistive Mitten (SSAM) [26], they use the deflection of leaf spring actuated by cable to mimic finger curling motion. But the finger curling joint angles were just estimated based on the model of cantilever deflection of the leaf spring and it generates continuous bending angle on the whole finger, not each joint of a finger, which means the device may not fit naturally with human fingers. By contrast, the spring blades in the three-layered sliding spring (TLSS) mechanism are constrained in the rigid frame to fit with human hand [24,25], which makes the mechanism achieve higher compatibility and adaptivity in a sleek design. Bent spring blades also can store energy, which is more applicable for post-stroke patients who suffer from hand spasticity to help them open their hands easily in the early stage of rehabilitation after stroke. However, most hybrid soft-rigid hand exoskeletons still lack a well-understood model to achieve comprehensible kinematics.

In this paper, we introduce a hybrid soft-rigid hand exoskeleton (HSRexo) adopting a simplified three-layered sliding spring (sTLSS) mechanism. Thanks to the elasticity of spring blades, this mechanism has better compliance compared with traditional purely rigid mechanisms. Due to the constraint of rigid parts, the sTLSS mechanism can be modeled by the pseudo-rigid-body model (PRBM) method with a satisfying accuracy compared with mechanisms entirely made of soft elastomer or cable-driven textiles. Finally, the simulation and the preliminary prototype are implemented to test the design and modeling of the HSRexo with the sTLSS mechanism.



## 2. Modeling and optimization of simplified three-layered sliding spring (sTLSS) mechanism

### 2.1. Modeling of sTLSS mechanism

The TLSS mechanism shown in Fig. 1(a) consists of spring blades (upper, middle, and bottom springs as Su, Sm, and Sb, respectively) and rigid bodies (holder and slider rigid parts as Rh and Rs, respectively). The bottom spring (Sb) of distal interphalangeal joint (DIP), proximal interphalangeal joint (PIP), and metacarpophalangeal joint (MCP) are fixed to the rigid holders (Rh) on distal phalanges (DP), middle phalanges (MP), proximal phalanges (PP) and metacarpal (MC), and mimic the bending of finger motion. The middle spring (Sm) blades are active ones that are bonded with the central rigid sliders (Rs) and the driver. The rigid slider plays a force transmission role when it moves in the rigid holders with the input linear movement from the back of the hand. The upper spring (Su) blades are passive ones that slide in a limited length of the rigid holders and play a role of limit in finger movements to ensure safety. In our sTLSS mechanism design used by HSRexo shown in Fig. 1(b), the rigid sliders in MP and PP holder (i.e., Rs<sub>1</sub>, Rs<sub>2</sub> in Fig. 1(a)) are abandoned. The middle spring is a whole spring blade. Compared with TLSS, the sTLSS mechanism has two main benefits: first, there is no friction with large-area contact between sliders and holders, which will reduce the required input force from the motion input and motors. Therefore, this will be good for the lightweight of the whole system. Second, this design will improve the conciseness of the mechanism fabrication because it is difficult to assemble spring blades and sliders in a limited space. This mechanism will make it easy to achieve a detachable function. Using one whole middle spring, we also do not need to determine the division of spring length for every joint of a finger, which will reduce the difficulty of custom-tailored mechanisms for different patients.

Because the sTLSS mechanism contains spring blades as highly elastic elements and rigid parts as constraints, it can be adapted to a human finger, as shown in Fig. 1(c). It is a typical compliant mechanism using nonlinear large-deflection elastic deflection to translate or convey movement, force, or energy. The compliant mechanism is playing more and more important roles in bionic mechanisms and robotics. That's mainly because its main advantages of reducing the cost (e.g., reduce the number of components, fabrication, and assembly time) and improving the performance (e.g., improve accuracy and reliability, reduce friction, weight, and maintenance, and store energy).

On the other hand, due to the nonlinear large deflection of compliant mechanism, the nonlinear equation of Bernoulli-Euler beam theory without small deflection assumption is needed to analyze the elastic deflection. But this will become a challenge if the compliant mechanism

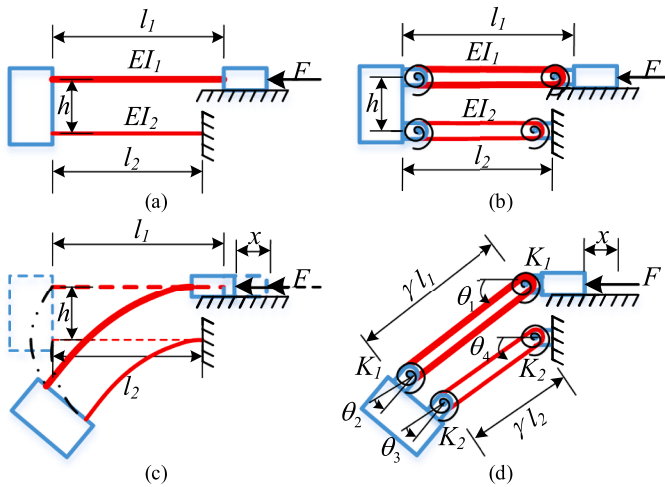


**Fig. 2.** Model of sTLSS mechanism. (a) A joint of sTLSS mechanism. (b) The PRBM of sTLSS joint. (c) Bent sTLSS joint. (d) Bent PRBM of sTLSS joint and its parameters representation.  $l_i$  is the length of spring blade;  $h$  is the distance between middle and bottom spring blades;  $K_i$  is the spring constant of torsional springs on hinge joints, and  $\theta_i$  is the angle of hinge joint (For interpretation of the references to color in this figure, the reader is referred to the web version of this article).

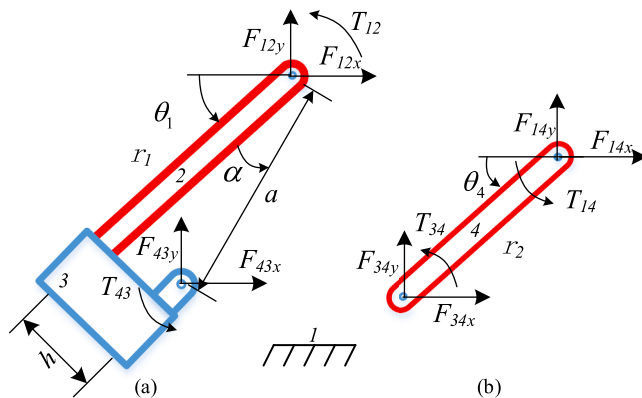


**Fig. 3.** Free body diagram of sTLSS mechanism derived from Fig. 2(d) when assuming  $\theta_2 = 0$ .  $F_{ij}$  and  $T_{ij}$  mean the force and spring torsion of component  $i$  exerted on  $j$ ; Component 1 represents the ground; The  $a$  and  $\alpha$  represent the distance and angle shown in (a), respectively.

is more complex like the sTLSS mechanism. Therefore, in this paper, we use the pseudo-rigid-body model (PRBM) method [27] to model the kinematics of sTLSS mechanism in a more simplified but still relatively accurate way, because the PRBM method can let us use the equivalent force-deflection relationships of rigid bodies to simulate that of compliant mechanisms.

In the PRBM method, the movement, trajectory, and force-deflection relationships of every compliant segment can be simulated by a rigid link with hinge joint and torsional spring attached on the joint [27]. In every joint of the sTLSS mechanism, the compliant segments (*i.e.*, spring blades shown in red) are all fixed-fixed segments in Fig. 2(a) and (c), which can be simulated by a rigid link with 2 hinge joints and 2 torsional springs on its two ends as shown in Fig. 2(b) and (d). In this case, characteristic radius factor  $\gamma = 0.85$  and stiffness coefficient  $K_\theta = 2.65$  [27]. Then the characteristic radius  $r_i$  is:

$$r_i = \gamma l_i, (i=1,2) \quad (1)$$

According to the geometric relationship in Fig. 2(d), the sTLSS mechanism is under constraint and does not have only one determination solution. Hence, we assume  $\theta_2 = 0$  as shown in Fig. 3(a), which is

the free body diagram derived from Fig. 2(d). According to the projection in respective directions, we can get the vertical and horizontal kinematics formulas, respectively:

$$\begin{cases} r_2 \sin \theta_4 + h = a \sin(\theta_1 + \alpha) \\ r_2 \cos \theta_4 + l_1 - l_2 + \frac{1-\gamma}{2} l_2 = a \cos(\theta_1 + \alpha) + (1-\gamma) l_1 + x \\ \theta_1 = \theta_3 + \theta_4 \end{cases} \quad (2)$$

where

$$\begin{cases} a = \sqrt{h^2 + \left(r_1 - \frac{1-\gamma}{2} l_2\right)^2} \\ \alpha = \arcsin\left(\frac{h}{a}\right) \end{cases} \quad (3)$$

The  $a$  and  $\alpha$  represent the distance and angle shown in Fig. 3(a), respectively. They are used for the conciseness of Eq. (2).

Therefore, the relationship between  $\theta_1$  and  $\theta_4$  is:

$$\theta_4 = \arcsin\left(\frac{\sin(\theta_1 + \alpha) - h}{r_2}\right) \quad (4)$$

Then, the motion relationship between  $\theta_1$  and required input displacement  $x$  is:

$$x = r_2 \cos \theta_4 - a \cos\left[\theta_1 + \arcsin\left(\frac{h}{a}\right)\right] + \gamma l_1 - \frac{1+\gamma}{2} l_2 \quad (5)$$

Besides, because we assume  $\theta_2 = 0$ , the upper spring blade is represented by a rigid link (link 2 in Fig. 3) and a single hinge joint with a single torsional spring on it. This segment is seen as a cantilever. But the bottom spring blade is still simplified as a fixed-fixed segment, which can be simulated by a rigid link (link 4 in Fig. 3) with 2 hinge joints and 2 torsional springs on its two ends. It can be seen as two connected symmetrical half-arm cantilevers. Their arms are both  $\gamma l_2/2$ . Therefore, the spring constant of torsional springs  $K_1$  is:

$$\begin{cases} K_1 = \gamma K_\theta \frac{EI_1}{l_1} \\ K_2 = 2\gamma K_\theta \frac{EI_2}{l_2} \end{cases} \quad (6)$$

where  $E$  is Young's modulus of the material of spring blade and the moment of inertia of spring blade  $I_i$  can be achieved by:

$$I_i = \frac{w_i t_i^3}{12} \quad (7)$$

where  $w_i$  is the width of spring blades,  $t_i$  is the thickness of spring blades.

According to the free body diagram in Fig. 3, we can get static balance equations from the middle spring blade (component 2) and mobile rigid part (component 3):

$$\begin{cases} F_{12x} + F_{43x} = 0 \\ F_{12y} + F_{43y} = 0 \\ T_{12} + T_{43} - F_{12x} \sin(\theta_1 + \alpha) + F_{12y} \cos(\theta_1 + \alpha) = 0 \end{cases} \quad (8)$$

where

$$\begin{cases} T_{12} = -K_1 \theta_1 \\ T_{43} = -K_2 \theta_3 \\ F_{12x} = -F \end{cases} \quad (9)$$

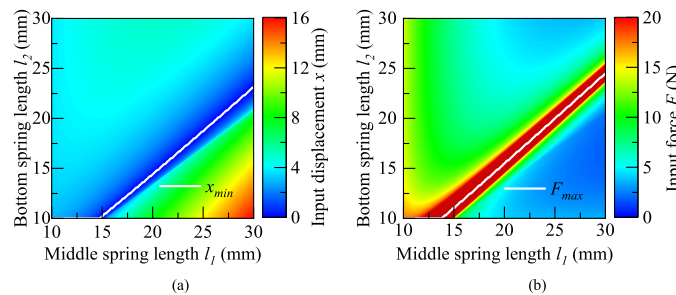
We can get static balance equations from the bottom spring blade (component 4):

$$\begin{cases} F_{34x} + F_{14x} = 0 \\ F_{34y} + F_{14y} = 0 \\ T_{34} + T_{14} - F_{14x} r_2 \sin \theta_4 + F_{14y} r_2 \cos \theta_4 = 0 \end{cases} \quad (10)$$

**Table 1.**

Parameters of index finger\*.

Variable (unit)	Value (DIP/PIP/MCP)	Variable (unit)	Value (DIP/PIP/MCP)
$w_1$ (mm)	(2/3/4)	$w_2$ (mm)	(5/5/6)
$t_1$ (mm)	(0.2)	$t_2$ (mm)	(0.1)
$l_1$ (mm)	(11/18/27)	$l_2$ (mm)	(10/17/26)
$\Gamma$	0.85	$K_\theta$	2.65
$E$ (GPa)	197	$h$ (mm)	2.45
$n$ (mm)	(1)		

\*Value in brackets is the result after optimization,  $n = l_1 - l_2$ ,  $n > 0$ .**Fig. 4.** The effect of the length of spring blades in sTLSS model on (a) required input displacement  $x$  and (b) required input force  $F$ .

where

$$\begin{cases} T_{34} = K_2 \theta_3 \\ T_{14} = -K_2 \theta_4 \end{cases} \quad (11)$$

Combining Eqs. (2), (8)–(11), and solving for required input force  $F$  yields:

$$F = \frac{\frac{K_1 \theta_1 + K_2 (\theta_1 - \theta_4)}{\alpha \cos(\theta_1 + \alpha)} + \frac{K_2 (2\theta_4 - \theta_1)}{r_2 \cos \theta_4}}{\tan(\theta_1 + \alpha) - \tan \theta_4} \quad (12)$$

According to these equations of the sTLSS model, we can get the

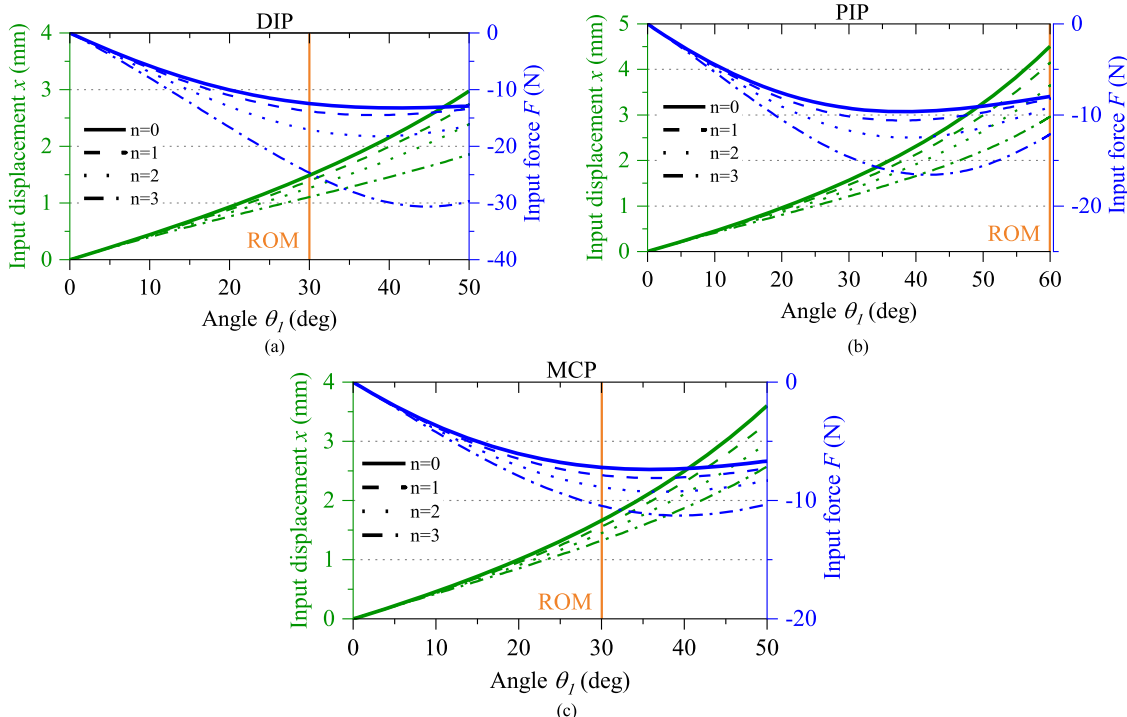
kinematics and relationship between joint angle, input displacement, and input force. This model can realize the quantitative description of the sTLSS mechanism and makes design optimization possible. We can get the effect of mechanical parameters to optimize the sTLSS mechanism by the model.

## 2.2. Optimization of sTLSS mechanism

First of all, there are several objectives for the optimization: (1) we choose DIP/PIP/MCP = 30°/60°/30° as the desired range of motion (ROM) of every joint because the angle requirement of the full ROM of the index finger is 120°, the full range of PIP is around 60° [25], and there is an around 2:1 coupled ratio of PIP and DIP [28]; (2) The sTLSS mechanism can avoid singularity. Singularity means that the mechanism is completely unable to move no matter how high the input force is; (3) We hope that the space occupied by input displacement of the whole finger is no more than 7 mm long (*i.e.*, lower input displacement  $x$ ), as well as the motors required by input force, are more portable (*i.e.*, lower input force  $F$ ).

Therefore, for objective (1), we repeat the modeling and preliminary finite element analysis (FEA) on the sTLSS mechanism varying the length, width, and thickness of spring blades in an about 0.5x–2x range of the desirable sizes mentioned in the former research [25] to compare the changes and obtain a desirable motion of finger joints. The width and thickness of middle and bottom spring blades, as well as the size and passive sliding limit of upper spring blades, are obtained to achieve desirable motion according to preliminary FEA. Taking the index finger as an example, the related parameters are shown in Table 1. After achieving the objective (1), we get all size parameters of spring blades except the length of middle and bottom spring blades.

Then for objective (2), we repeat the modeling analysis varying the length of middle and bottle spring blades. The effect of the respective length  $l_i$  of middle and bottom spring blades on the required input displacement  $x$  and input force  $F$  is calculated by Eqs. (5) and (12) and shown in Fig. 4(a) and (b). The sTLSS mechanism meets singularity at the same structure parameter where the input displacement  $x$  is approaching 0 (*i.e.*,  $x_{min}$ ) and the input force  $F$  is approaching infinity (*i.e.*,

**Fig. 5.** Modeling results of (a) DIP, (b) PIP, and (c) MCP. The ROM means full range of motion of joints.

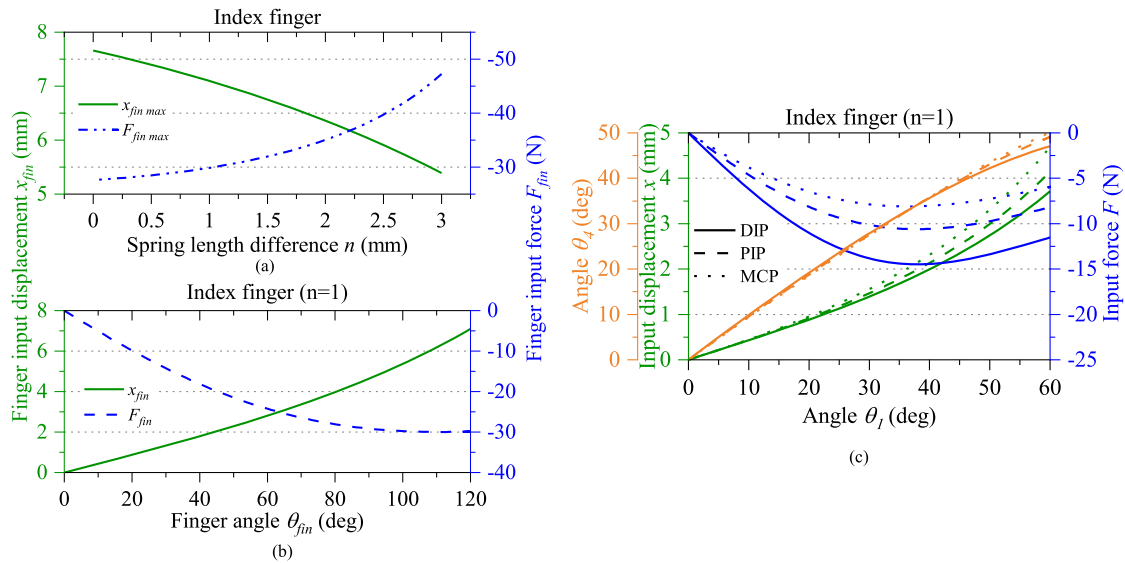


**Fig. 6.** Modeling results of index finger. (a) The effect of spring length difference. (b) The modeling results of whole index finger when spring length difference  $n$  is 1. (c) The modeling results of every joint in index finger when spring length difference  $n$  is 1.

etc.,  $F_{max}$ ). This also demonstrates the consistency of the modeling method. In this case, we can see that  $x_{min}$  and  $F_{max}$  are both shown in the approximately same line with a gradient of 1 where the length difference  $n$  ( $l_1 - l_2$ ) between middle and bottom spring is around 5. Therefore, the range of  $n > 4$  should be avoided in the choice of  $n$ . Besides, other value also shows the similar gradient when the difference  $n$  is around 0–3. It means the simultaneous change of length of middle and bottom spring has less effect on the required input displacement  $x$  and input force  $F$ , but the length difference  $n$  plays a major role in this range.

For objective (3), the required input displacement  $x$  and force  $F$  of DIP, PIP, and MCP joint of the index finger when  $n = 0$ –3 are calculated by Eqs. (5) and (12) and shown in Fig. 5. Both  $x$  and  $F$  have a nonlinear relationship with angle  $\theta_1$ , which can be approximately seen as the joint angle. Besides, along with the increase of length difference  $n$ , the required input displacement  $x$  decreases, and the force  $F$  increases in every index finger joint.

Fig. 6 (a) shows the maximum sum required input  $x$  and  $F$  of the whole index finger in case of the desired ROM. The  $x$  changes between around 5.5 and 7.5 mm, but the  $F$  changes between around 30 and 50 N, which is more significant for the choice of  $n$ . As a result, in consideration of the tradeoff between  $x$  and  $F$ , we choose  $n = 1$  mm in our design where  $F = 30$  N is relatively low and  $x = 7$  mm is allowed under the requirement of objective (3). Due to the optimization of  $n$ , we can reduce the input force of the mechanism and the space required by input displacement.

As shown in Fig. 6(b), we can get the finger input displacement  $x_{fin}$  and finger input force  $F_{fin}$  changing along with the finger angle  $\theta_{fin}$ , if we assume that three joints of the index finger deform at the same time with the same speed of changing percentage of individual ROM according to the nonlinear kinematics of every joint shown in Fig. 6(c). The finger angle  $\theta_{fin}$  is the sum of the three joint angles in the finger, which is also the overall flexion angle of the finger. The required finger input displacement is about 7 mm, and the sum of the required input force of a finger needs to be around 30 N in our modeling result in Fig. 6(b). In the former TLSS mechanism, Bützter et al. have conducted experiments on the mechanism and the input force of a finger is around 30 N at an overall finger flexion angle of 90° when the fingertip force keeps ON [24], which accords with our modeling result in Fig. 6 (b).

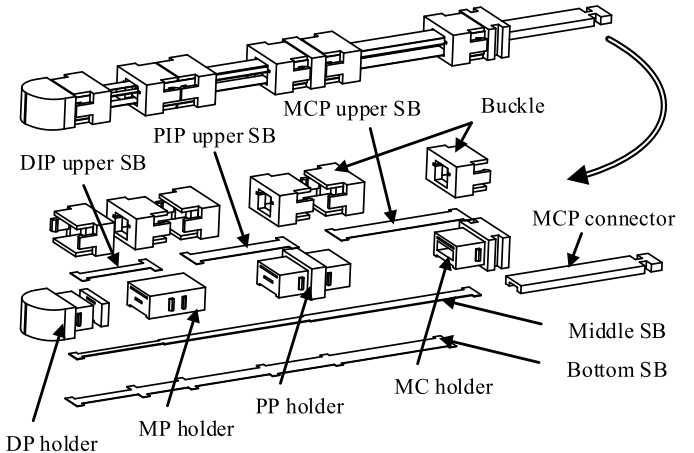


**Fig. 7.** Exploded view of finger module. "SB" means "spring blade".

### 3. Mechanical design of the hand exoskeleton

#### 3.1. Finger module design

The HSRExo hand exoskeleton contains two modules: finger module and palm module. The finger module shown in Fig. 7 contains four holders, three joints using three-layer spring blades between them as an STLSS mechanism, 6 buckles for constraint and fixing purposes, and an MCP connector as motion input. Four holders are distal phalange (DP) holder, middle phalange (MP) holder, proximal phalange (PP) holder, metacarpal (MC) holder, respectively. Spring blades (SB) are bottom spring blade, middle spring blade, DIP/PIP/MCP upper spring blade. Phalange holders are correspondingly connected on the human finger and hand by hook & loop fasteners. MC holder is connected to the palm module. The bottom spring blade is fixed with each phalange holder and MC holder. The middle spring blade is fixed on the DP holder with one side, runs through the MP/PP/MC holders, and then fixed on the MCP connector with another side. The DIP/PIP/MCP upper spring blade is fixed on the DP/MP/PP holder with one side, and another side can passively slide in the limit of the MP/PP/MC holder, respectively. All the fixing and limit constraints are realized by the 6 buckles, which are designed to achieve detachable.

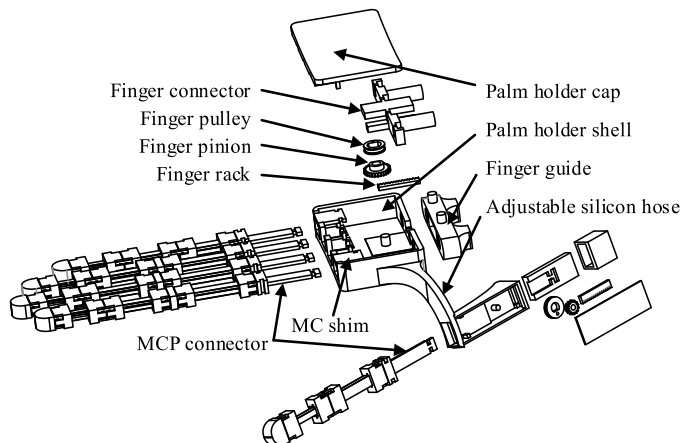


**Fig. 8.** Explosive view of palm module.

In this way, the MCP connector moves forward and then takes the middle spring blade to move forward. The distances between holders increase. The upper spring blades slide in the respective limit of holders. But because the bottom of every holder is fixed by the bottom spring blade, so the whole finger module is bent by the motion of the MCP

connector under the constraint of the bottom spring blade. When the joints reach desired angle, every upper spring blade arrives at the endpoint of the respective limit to make sure the safety of patients wearing the exoskeleton. As a result, the finger module can realize the flexion motion. When the MCP connector moves backward, the whole extension motion of the finger module is just the opposite of the flexion motion stated above. The thumb module is like the finger module but just has three holders and two joints between them.

### 3.2. Palm module design

The palm module shown in Fig. 8 plays a role in the motion input of finger modules. It contains a palm holder shell, palm holder cap, 2 metacarpal (MC) shim, adjustable silicone hose, thumb holder shell, and thumb holder cap. In hand rehabilitation training, the main goal is to realize the grasp motion of the hand. Therefore, we adopt an underactuated method that four fingers use one motion input end effector in a coupled relationship, and the thumb uses another because of its independence in the motion. Every end effector contains a finger connector, guide, rack, pinion, and pulley.

Specifically, the palm holder shell and thumb holder shell are connected by the adjustable silicone hose, and then both can be mounted on the human opisthenar by hook & loop fasteners. The palm holder cap can cover the palm holder shell and together constrain the inner end

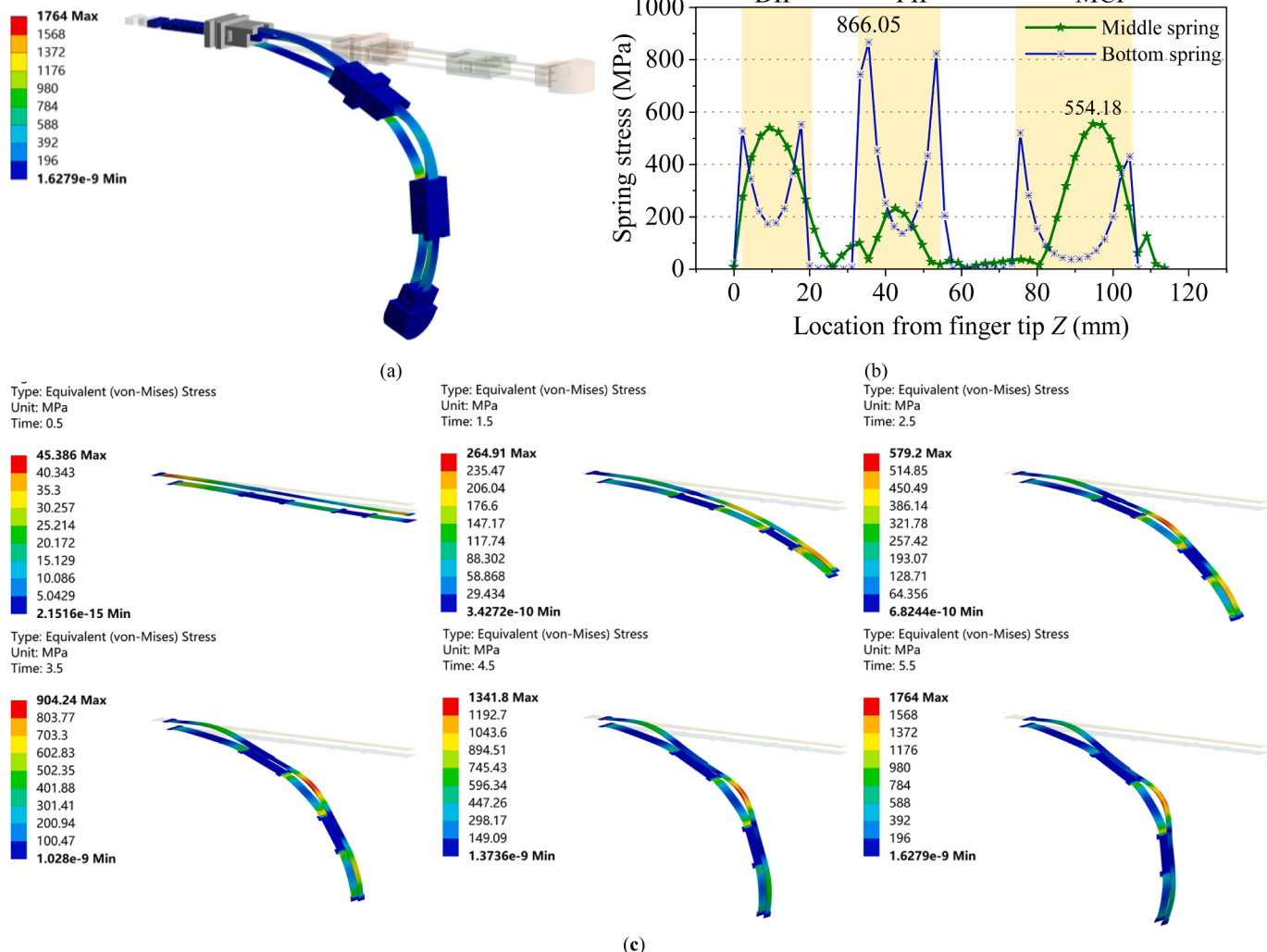


**Fig. 9.** Spring stress in simulation result of finger module. (a) The deformation of index finger. (b) The time series of deformation of middle and bottom spring. (c) The stress distribution of middle and bottom spring.

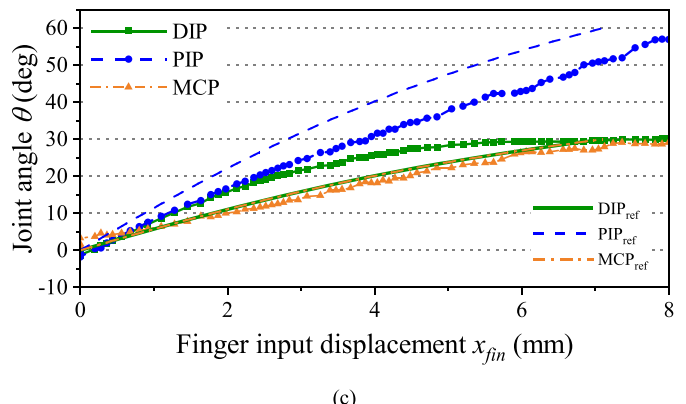
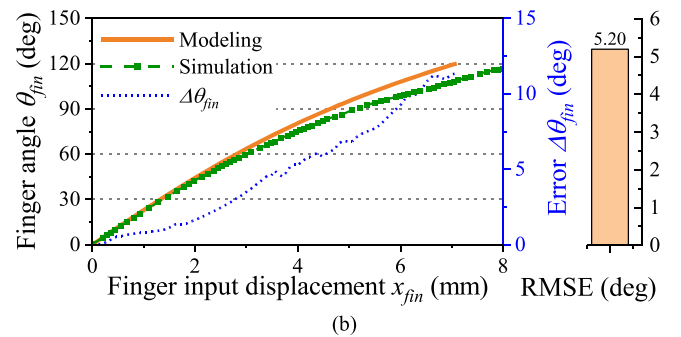
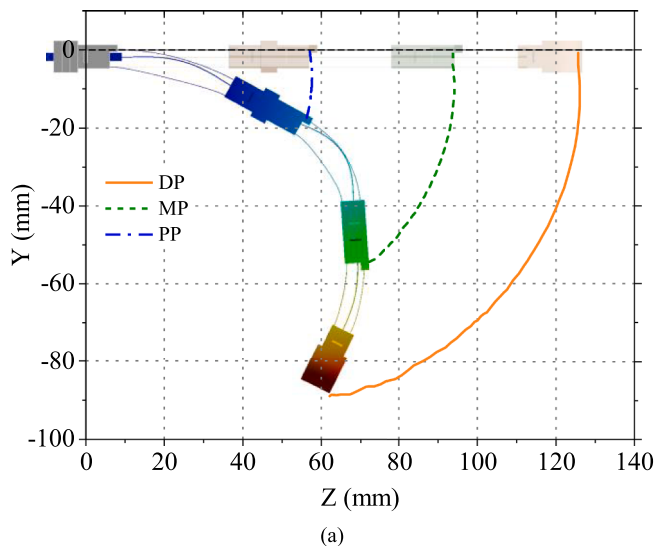


**Fig. 10.** Trajectory and angle in simulation result of finger module. (a) Trajectory of finger joints. (b) Finger angle  $\theta_{fin}$  corresponding to the overall spring displacement of finger  $x_{fin}$  and its error relative to modeling result. (c) Joint angle referring to modeling result.

effector of four fingers. Regarding the end effector, the finger connector in the palm module is fixed with the MCP connector in the finger module. The guide for four fingers is fixed on the wrist side of the palm holder shell and can guide the linear motion of the finger connector by the guide rail. The rack is constrained by the finger connector and engages with the pinion that has a fit with the pulley by a D shaft. The end effector for the thumb is almost the same structure as that for four fingers.

In this way, the cable on the pulley can drive the pulley and pinion to rotate. The rotation can be transferred to linear motion by pinion and rack. Then the rack drives the finger connector to move back and forth. The finger connector then can drive four MCP connectors simultaneously as input motion of four finger modules. Likewise, the thumb part is almost the same. In our design, Bowden cable makes the remote arrangement of actuators possible and lightens the weight of the wearable part of the hand exoskeleton.

#### 4. Simulation and preliminary prototype testing

##### 4.1. The simulation of finger flexion and extension

We use finite element analysis (FEA) software to simulate the motion of sTLSS without payload. The simulation process is divided into two steps: first, the standard Earth gravity is gradually loaded within the initial 0.5 s. Second, the MCP connector advances 8 mm between 0.5 and 5.5 s. The displacement in the simulation (8 mm) is more than the required input displacement in the modeling result (around 7 mm in Fig. 6(b)) to make sure it covers the whole range of motion input. The mesh element size is 0.6 mm. The meshing method of spring blades is Sweep. Large deflection is on. The frictional coefficient is 0.2 for frictional contact. The normal stiffness is set as absolute value at 1 N/mm<sup>3</sup>.

The simulation result in Fig. 9(a) shows the deformation of the finger module at the end time (5.5 s), and the time series of the simulation result of middle and bottom spring blades are shown in Fig. 9(c), which

are similar to human finger flexion motion. We choose testing paths on the middle and bottom spring blades to get the stress distribution when it is on the largest deformation status at 5.5 s, shown in Fig. 9(b). The stress of the middle spring is mainly concentrated on the DIP and MCP joints. The stress of the bottom spring is mainly concentrated on the PIP joint. The maximum stress of the bottom spring of every joint occurs on the boundary line of contact with every rigid part (*i.e.*, phalange holder). The overall largest stress 866.05 MPa occurs on the bottom spring of the DIP joint, which is smaller than the referenced permissible bending stress 1072.5 MPa.

The trajectory of every phalange holder in the simulation is shown in Fig. 10(a), which is also similar to the natural flexion-extension of a human finger. When the angle of the finger module is about 120 ° measured by the DP holder, the input displacement needs to be 8 mm as shown in Fig. 10(b), which is a little more than the modeling result at around 7 mm in Fig. 6(b). Before the finger angle  $\theta_{fin}$  reaches 100 °, the error of finger angle ( $\Delta\theta_{fin}$ ) between modeling and simulation in Fig. 10(b) keeps lower than 10 ° and increases with the finger angle. The maximum error is around 11 °, which only occurs at the maximum ROM. This demonstrates that the model has worse accuracy at around maximum ROM. To have an overall view of the accuracy, we use the root mean square error (RMSE) to calculate:

$$RMSE = \sqrt{\frac{\sum_i^m \Delta\theta_i^2}{m}}. \quad (13)$$

The RMSE here is low at 5.20 °. This can cogently demonstrate the overall accuracy of the sTLSS model.

However, we found that there are certain changes of speed and difference of ROM occurring in the deformation of three joints, though the three joints start the deformation at the same time. Fig. 10(c) shows the joint angle of three joints in the simulation result referring to the individual deformation of every joint in the modeling result. At the beginning of finger flexion, the DIP joint deforms at a relatively high speed,

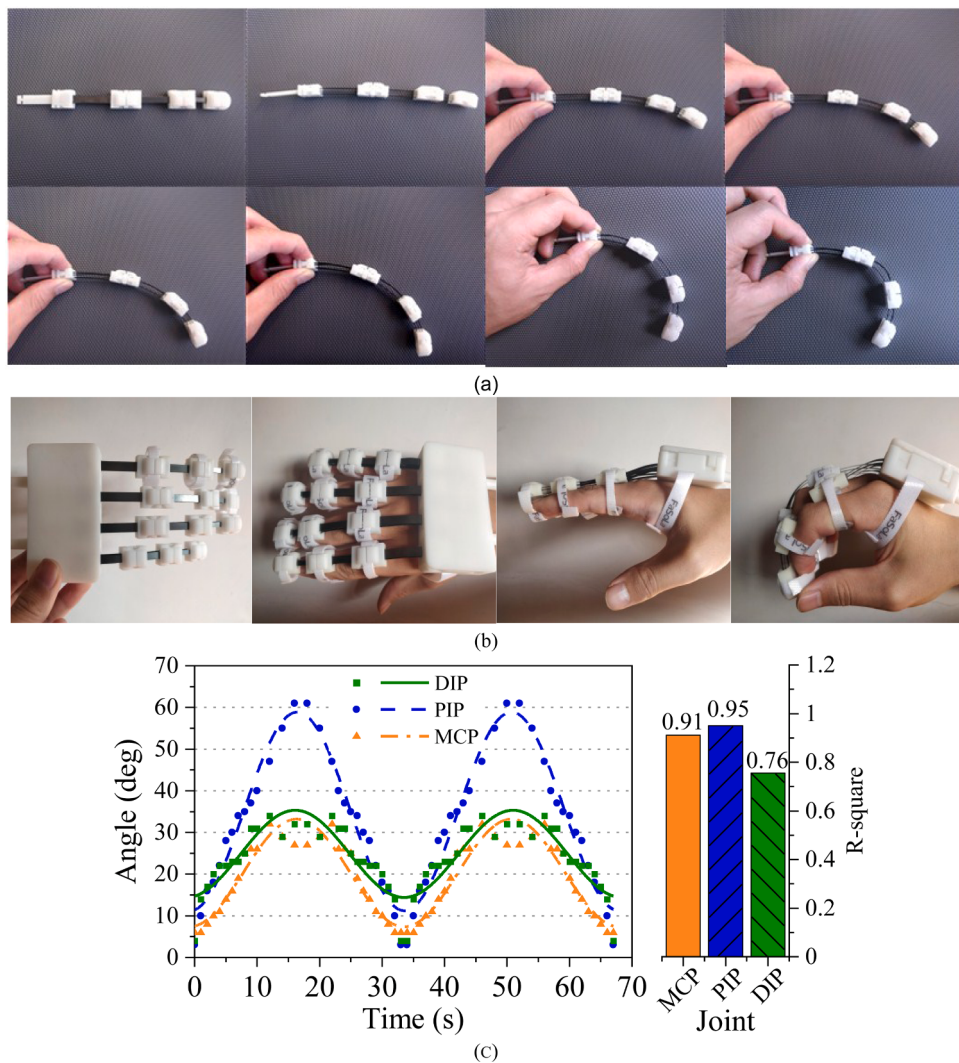


**Fig. 11.** Result of preliminary prototype. (a) Motion evaluation of finger prototype. (b) Preliminary prototyping of HSRexo worn on a user. (c) Evaluation results of finger angle.

but the deformation speed of DIP slows down at the end of finger flexion. So, the ROM of DIP is almost the same as the referenced modeling result. The deformation speed through the whole finger flexion, as well as the final ROM of the MCP joint, are both almost consistent with referenced modeling result. However, the PIP joint deforms at relatively low speed, and a slight reduction of ROM occurs at around 10°, which is responsible for the error of finger angle between modeling and simulation in Fig. 10 (b). Although this consequence of the change in deforming speed of the DIP joint may not affect subjects due to the adaptation of spring blades, it as well as the difference of ROM of PIP joint still should be further researched in the future to achieve better understanding.

#### 4.2. Preliminary prototype implementation and evaluation

In the preliminary prototype, the spring blades are 65Mn steel strips. Other rigid parts are 3D-printed acrylonitrile-butadiene-styrene (ABS) resin. Therefore, the HSRexo hand exoskeleton can be light, cheap, and easy to customize. The weight of finger and palm modules is only around 100 g. Besides, due to the simplified and detachable design, the assembly, interchangeability, and replacement of tailored parts can be more convenient.

The time series of the finger module in motion are shown in Fig. 11 (a), in which the MC holder is fixed on the desk and input displacement is exerted on the MCP connector. The preliminary prototyping worn on a

user is shown in Fig. 11(b). The burden from HSRexo on the user's hand is low, the user can move the hand with HSRexo freely and perform grasp motion of hand naturally.

We measure the joint angles in time series to get the change of angle over time shown in Fig. 11(c) and make a suitable extension of the curve for fitting. We can see that the maximum angles of the MCP/PIP/DIP joint are 32°/61°/34°, respectively, which can almost satisfy the 30°/60°/30° angle requirement and the 2:1 coupled ratio of PIP and DIP.

In our former research, we have collected the angle data of healthy subjects' fingers by angle sensors in a mature finger exoskeleton. It showed that the natural flexion/extension trajectory of the finger joint is approximately a sine curve with an R-square value at  $0.96436 \pm 0.0089$  [28]. The R-square value is used to evaluate the goodness of fitting. It is generally believed that the R-square over 0.8 is relatively high enough. The closer the R-square value is to 1, the better the fitting goodness is, which means the closer the joint angle of the exoskeleton is to the natural flexion/extension of a finger joint.

Therefore, we use a sine curve to fit the angle change here. In Fig. 11 (c), both the MCP and PIP joints have a good fitting with an R-square value greater than 0.9, indicating that the MCP/PIP joint angles are very close to natural motion. The R-square value of DIP is a little lower than 0.8. The reasons may be that the DIP joint is far from the motion input and the spring blades of DIP joint are shorter. They jointly lead to the motion constraint of the DIP joint around the extreme angle. Because

there is coupled relation between DIP and PIP joints of a human finger, the DIP motion has less effect on the hand motion, and the compliant sTLSS mechanism can adapt to the human finger, we think the result is acceptable if we give DIP more tolerance in front of the advantage of sTLSS mechanism.

## 5. Conclusion

In this paper, a hybrid soft-rigid hand exoskeleton (HSRexo) adopting a simplified three-layered sliding spring (sTLSS) mechanism is proposed for hand rehabilitation after stroke. The compliant spring blades in the sTLSS mechanism make it possible to compactly actuate three natural flexion/extension of finger joints by only 1-DOF. The simplified and detachable design can reduce the friction between sliders and holders, improve the conciseness of the mechanism fabrication, and enhance the convenience of patients' daily use as well, but still has the same performance as the former design. To deal with the nonlinear deformation problem of soft elastic elements, the kinematic modeling of the sTLSS mechanism is presented by the pseudo-rigid-body model (PRBM) method to achieve comprehensible kinematics and optimize parameters of the mechanism.

Therefore, the HSRexo combines intrinsic compliance and comprehensible kinematics and has portable, wearable, and compliant advantages. The design can also reduce the cost and improves the applied range of the device in different clinical and home environments. Finally, the simulation and preliminary prototyping demonstrate the accuracy of the model and the compliant natural flexion/extension joint angle of the HSRexo design due to the modeling and optimization of the sTLSS mechanism.

For different applications, the PRBM method can largely reduce the difficulty of numerical analysis and optimization of compliant mechanisms using nonlinear large deflection. The application of the PRBM method in this paper is proved to instruct the optimization and design in the sTLSS mechanism. The sTLSS model may also have wide inspiration on modeling mechanisms using spring blades for compliant purposes.

However, there are still other problems or ideas that we need to

research in the future: (1) there is a slight slide between phalange holders and fingers during the motion because the bottom spring blades are fixed on the phalange holders, which needs more future research to improve the comfortability; (2) Designing and modeling the adduction/abduction motion of MCP joints and entirely prototyping the HSRexo; (3) The deformation speed changing of DIP and the difference of ROM of PIP between modeling and simulation; (4) Conducting clinic experiment on patients surviving from stroke and more optimization on the device according to the clinic experiment results. Finally, we aim to realize a more scientific and humane hand rehabilitation using this HSRexo hand exoskeleton.

## CRediT authorship contribution statement

**Legeng Lin:** Conceptualization, Methodology, Software, Validation, Formal analysis, Investigation, Data curation, Writing – original draft, Writing – review & editing, Visualization, Project administration, Funding acquisition. **Fuhai Zhang:** Conceptualization, Resources, Supervision, Writing – original draft, Writing – review & editing, Project administration, Funding acquisition. **Lei Yang:** Software, Resources, Data curation, Funding acquisition. **Yili Fu:** Resources, Funding acquisition.

## Declaration of Competing Interest

The authors declare that they have no known competing financial interests or personal relationships that could have appeared to influence the work reported in this paper.

## Acknowledgment

This work was supported in part by the National Natural Science Foundation of China (Grant No. 62073097), the Natural Science Foundation of Heilongjiang Province of China (Grant No. LH2021F027), and Self-Planned Task (Grant No. SKLRS202107B) of State Key Laboratory of Robotics and System (HIT).

## Appendix

Table 2. List of symbols.

Symbol	Meaning	Symbol	Value (DIP/PIP/MCP)
$a$	Distance defined in Fig. 3(a)	$r_i$	Characteristic radius
$E$	Young's modulus	$T$	Spring torsion
$F$	Input force	$t_i$	Thickness of spring blade
$h$	Distance between middle and bottom spring blades	$w_i$	Width of spring blade
$I_i$	Moment of inertia	$x$	Input displacement
$K_0$	Stiffness coefficient	$\alpha$	Angle defined in Fig. 3(a)
$K_t$	Spring constant of torsional spring	$\gamma$	Characteristic radius factor
$l_i$	Length of spring blade	$\Delta\theta$	Error of angle
$n$	Length difference between middle and bottom spring		

Table 3. List of abbreviations.

Abbreviation	Meaning	Abbreviation	Value (DIP/PIP/MCP)
ABS	Acrylonitrile-Butadiene-Styrene	PP	Proximal Phalanges
ADL	Activities of Daily Life	PRBM	Pseudo-Rigid-Body Model
COR	Center Of Rotation	Rh	Rigid holder
DIP	Distal Interphalangeal joint	RMSE	Root Mean Square Error
DOF	Degree Of Freedom	Rs	Rigid slider
DP	Distal Phalanges	ROM	Range Of Motion
fDOF	functional Freedom Of Degree	SB	Spring Blades
FEA	Finite Element Analysis	Sb	bottom Spring
HSRexo	Hybrid Soft-Rigid exoskeleton	Sm	middle Spring
MC	Metacarpal	SSAM	Single-size Semi-soft Assistive Mitten
MCP	Metacarpophalangeal joint	sTLSS	simplified Three-Layered Sliding Spring
MP	Middle Phalanges	Su	upper Spring
PIP	Proximal Interphalangeal joint	WHO	World Health Organization

## References

- [1] World Health Organization. Stroke, Cerebrovascular accident: Health topics, <http://www.emro.who.int/health-topics/stroke-cerebrovascular-accident>; 2020 [accessed: 25 September 2021].
- [2] Basteris A, Nijenhuis SM, Stienen AHA, Buirke JH, Prange GB, Amirabdollahian F. Training modalities in robot-mediated upper limb rehabilitation in stroke: a framework for classification based on a systematic review. *J Neuro Eng Rehabil* 2014;11:111.
- [3] French B, et al. Repetitive task training for improving functional ability after stroke. *Stroke* 2009;40:e98–9.
- [4] Gopura R, Bandara D, Kiguchi K, Mann G. Developments in hardware systems of active upper-limb exoskeleton robots: a review. *Robot Auton Syst* 2016;75:203–20.
- [5] Bos RA, et al. A structured overview of trends and technologies used in dynamic hand orthoses. *J Neuro Eng Rehabil* 2016;13(1):62.
- [6] Fontana M, Dettori A, Salcedo F, Bergamasco M. Mechanical design of a novel hand exoskeleton for accurate force displaying. In: Proceedings of the IEEE international conference on robotics and automation; 2009. p. 1704–9. May.
- [7] Pu SW, Pei YC, Chang JY. Decoupling finger joint motion in an exoskeletal hand: a design for robot-assisted rehabilitation. *IEEE Trans Ind Electron* 2020;67(1):686–97. Jan.
- [8] Secciani N, Pagliai M, Buonomici F, Vannetti F, Volpe Y, Ridolfi A. A novel architecture for a fully wearable assistive hand exoskeleton system. *Mech Mach Sci* 2020;91:120–7.
- [9] Zhang F, Hua L, Fu Y, Chen H, Wang S. Design and development of a hand exoskeleton for rehabilitation of hand injuries. *Mech Mach Theory* 2014;73:103–16.
- [10] Jo I, Park Y, Lee J, Bae J. A portable and spring-guided hand exoskeleton for exercising flexion/extension of the fingers. *Mech Mach Theory* 2019;135:176–91.
- [11] Agarwal P, Yun Y, Fox J, Madden K, Deshpande AD. Design, control, and testing of a thumb exoskeleton with series elastic actuation. *Int J Robot Res* 2017;36(3):355–75.
- [12] Cempini M, Cortese M, Vitiello N. A powered finger-thumb wearable hand exoskeleton with self-aligning joint axes. *IEEE/ASME Trans Mechatron* 2015;20(2):705–16. Apr.
- [13] Polygerinos P, Wang Z, Galloway KC, Wood RJ, Walsh CJ. Soft robotic glove for combined assistance and at-home rehabilitation. *Robot Auton Syst* 2015;73:135–43.
- [14] Chen X, et al. A wearable hand rehabilitation system with soft gloves. *IEEE Trans Ind Inf* 2021;17(2):943–52. Feb.
- [15] HyunKi I, Cho KJ, Kim K, Lee B. Jointless structure and under-actuation mechanism for compact hand exoskeleton. In: Proceedings of the IEEE international conference on rehabilitation robotics (ICORR); 2011. p. 1–6. Jun.
- [16] Rus D, Tolley MT. Design, fabrication and control of soft robots. *Nature* 2015;521(7553):467–75. May.
- [17] Yue Z, Zhang X, Wang J. Hand rehabilitation robotics on poststroke motor recovery. *Behav Neurol* 2017;2017(3):1–20.
- [18] Cao Z, Xiao Q, Huang R, Zhou M. Robust neuro-optimal control of underactuated snake robots with experience replay. *IEEE Trans Neural Netw Learn Syst* 2018;29(1):208–17.
- [19] Zhong G, Dou W, Zhang X, Yi H. Bending analysis and contact force modeling of soft pneumatic actuators with pleated structures. *Int J Mech Sci* 2021;193:106150.
- [20] Chen L, Wang X, Xu WL. Inverse transmission model and compensation control of a single-tendon-sheath actuator. *IEEE Trans Ind Electron* 2014;61(3):1424–33. Mar.
- [21] Rose CG, O’Malley MK. Hybrid rigid-soft hand exoskeleton to assist functional dexterity. *IEEE Robot Autom Lett* 2019;4(1):73–80. Jan.
- [22] Wang D, Wang Y, Zi B, Cao Z, Ding H. Development of an active and passive finger rehabilitation robot using pneumatic muscle and magnetorheological damper. *Mech Mach Theory* 2020;147:103762.
- [23] Serbest K, Erdogan O. Design, development and evaluation of a new hand exoskeleton for stroke rehabilitation at home. *J Polyttech* 2021;24(1):305–14.
- [24] Bützter T, Lambery O, Arata J, Gassert R. Fully wearable actuated soft exoskeleton for grasping assistance in everyday activities. *Soft Robot* 2021;8(2):128–43.
- [25] Arata J, Ohmoto K, Gassert R, Lambery O, Fujimoto H, Wada I. A new hand exoskeleton device for rehabilitation using a three-layered sliding spring mechanism. In: Proceedings of the IEEE international conference on robotics and automation (ICRA); 2013. p. 3902–7. May.
- [26] Kaneishi D, et al. Design and assessment of a single-size semi-soft assistive mitten for people with cervical spinal cord injuries. In: Proceedings of the IEEE-RAS 19th international conference on humanoid robots (humanoids); 2019. p. 614–21. Oct.
- [27] Howell LL. Compliant mechanisms. NY, USA: John Wiley; 2001.
- [28] Zhang F, Lin L, Yang L, Fu Y. Variable impedance control of finger exoskeleton for hand rehabilitation following stroke. *Ind Robot* 2019;47(1):23–32.